DEFORMATION OF SANDY DEPOSITS BY REVERSE FAULTING

H. Taniyama[1] and H. Watanabe[2]

[1]MS, Research Assoc., Dept. of Civil and Environmental Eng., Saitama University
(Shimo-Okubo 255, Urawa, Saitama 338-8570, Japan, taniyama@goemon.dr5w.saitama-u.ac.jp)
[2]Dr. of Eng., Professor., Dept. of Civil and Environmental Eng., Saitama University
(Shimo-Okubo 255, Urawa, Saitama 338-8570, Japan, hiroyuki@post.saitama-u.ac.jp)

We performed sandbox tests and numerical analysis of the tests to investigate the deformation of the sand by reverse faulting. Test results can be simulated generally well by FEM using elasto-plastic solid elements and joint elements, if the stress-strain relation of the sand is adequately modeled. We applied our numerical model to prototypic real scale sandy alluvium model. The analyses of 30m, 50m and 75m deep alluvium suggested that the failure surface propagates through the alluvium if the vertical bedrock fault displacement reaches 3-7% of the depth of the alluvium. It is unlikely that the shear failure propagates through 100m deep alluvium.

Key Words : *earthquake fault, reverse fault, deposits, elato-plastic analysis, FEM*

1. INTRODUCTION

The understanding of earthquake fault rupture propagation through unconsolidated deposits overlying potentially active faults is important in planning structures near such faults. It is also important for mid term to long term earthquake prediction because recurrence period of earthquakes is often inferred by surface-faulting earthquakes.

Cole & Lade (1984) performed tests using dry sand and predicted the shape of the failure surface over dip-slip fault as a function of the depth of the soil, the angle of dilation for the soil, and the dip angle of the fault. Tani & Ueta (1991) modified Cole and Lade's formulation from the kinematic point of view.

Scott & Schoustra (1974) performed numerical simulation of 800m-deep alluvium over vertical fault by two-dimensional finite element method (FEM) assuming a linear-perfectly plastic relation. Their results showed the rupture zone bending over to the upthrown side, which is not consistent with experimental results. Roth et al., (1982) compared the centrifuge tests and the shear rupture in 6m deposits with their finite difference simulation and concluded the simulation could duplicate the experiments qualitatively.

Walters & Thomas (1982) performed sandbox experiment and conducted numerical simulation of their experiment by FEM. They found that nonassociated flow rule and strain softening were essential in localization of rupture. But in their FE analysis, rupture propagated through the sand and broke the ground surface with only a fraction of the displacement observed in experiments.

Bray et al., (1994) performed FE analyses and compared the results with the clay-box experiments and anchor pull-out experiments. They showed that numerical analyses could simulate experimental results quantitatively well, provided that soil's nonlinear stress-strain relation was adequately modeled.

Tani (1994) performed sandbox tests and FE analyses. He showed the importance of modeling discontinuous behavior of failure surface in analyzing the post failure process as well as the process before rupture. He showed the joint element was useful for this purpose.

In this paper, we present our sandbox test results and numerical model for simulating the test. Sandbox tests were performed to show the deformation and shear failure development in sand subjected to reverse faulting. We performed FEM
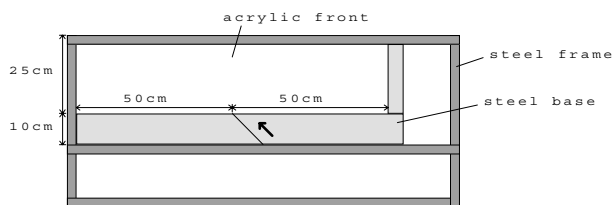
Figure 1: Apparatus for sandbox test

analysis of our test utilizing elasto-plastic theory to model nonlinear stress-strain relation of the sand and the joint element to model failure surface of the sand. Then we apply our numerical model to prototypic real scale alluvium model calculating the dynamic movement of bedrock fault by dynamic FE analysis.

2. SANDBOX TEST AND NUMERICAL SIMULATION

2.1 Sandbox test

The apparatus for sandbox tests shown in Figure 1 consisted of steel base (100 cm long and 20 cm wide) and acrylic sidewall (100cm long and 25cm high). The steel base was divided in half (50cm long). One half of them was fixed and the other half could be moved up at 45 degree relative to the fixed one.

Gifu sand (average grain diameter 0.33mm, uniformity coefficient 1.59) was packed in the test apparatus by dropping from 1m above the base steel. Red ink-stained dry sand was added at every 3cm height as a marker. As the base fault moved up by using a hydraulic jack, the packed sand deformed and the shear failure surface developed.

Typical test results are shown in Figure 2. Figure 2a shows the sand mass in the undeformed condition. The height (depth) of the sand was 17.5cm and the density of the sand was 1.59g/cm^3. Shear wave velocity (110m/s) was obtained at the depth of 10cm.

The sand starts to deform in the lowest part near the base fault (Fig. 2b). The shear failure develops upward with an increase in base displacement and it bends over to the footwall side as it approaches to the ground surface (Fig. 2c, 2d). The failure surface broke the ground surface when the vertical component of the base fault displacement was 8mm (4.1% of the depth of the sand). The deformation of the sand in the footwall side was observed mostly in the region near the shear failure surface and marker lines in the footwall show that they were dragged upward by the hanging wall. The deformation in the hanging wall side is small and widespread.
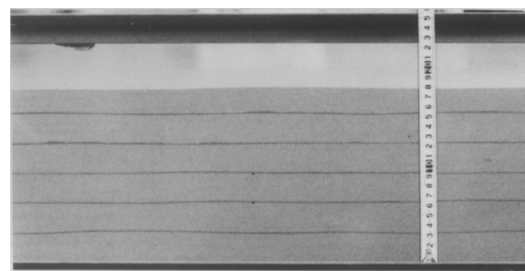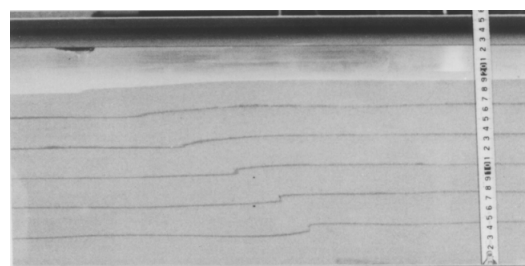

(a) initial state
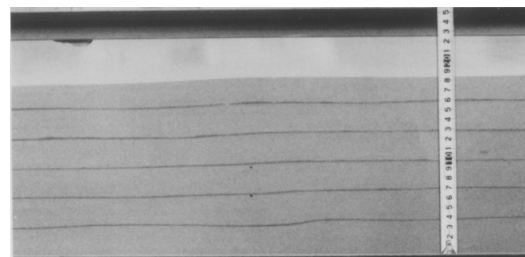
(b) vertical component of displacement 5mm
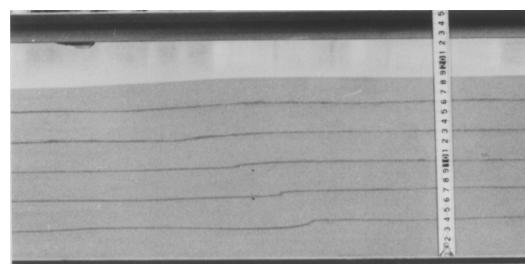
(c) vertical component of displacement 8mm

**(d) vertical component of displacement 12mm**

Figure 2: Deformation of sand

Once the shear failure surface reaches the ground surface, the deformation occurs mostly near this failure surface (Fig. 2d).

For the other four experiments we performed, the same deformation pattern of the sand was observed although the location of the failure surface was slightly different from each other. The vertical component of the base fault displacement needed to break the ground surface was within the rage of 7mm-9mm corresponding to 4%-5% of the depth of

Table 1: Parameters of numerical analysis

			Solid element	Joint element
Initial shear modulus		G_0	Equation (4)	Equation (4)
Poisson's ratio		ν	0.3	
Density			1.59g/cm^3	
Parameters of Mohr-Coulomb criterion	Cohesion	C		0.0Pa
	Friction angle	ϕ		51.4 degree
Parameters of Drucker-Prager criterion		α	0.27	
		k	0.0Pa	
Hardening function parameters		D	0.002(kN/m^2)$^{-1}$	
		W	0.15	
Major axis/minor axis		R	3.1	
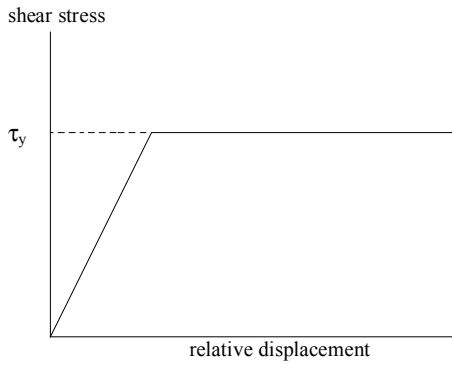
Figure 3: Constitutive relation of joint elements

the sand, which is compatible with the result of Cole & Lade (1984) (4%) and Tani (1994) (3%-6%).

2.2 Numerical simulation of sandbox test

We simulated our test result by FEM. Plane strain isoparametric rectangle and triangle elements were used for solid elements. The shear failure surface was modeled by joint elements (Toki & Miura, 1985). Shear stress-relative displacement relation in joint elements is assumed to be elastic-perfectly plastic (Fig. 3). The shear strength (τ_y) was obtained by Mohr-Coulomb criterion. The location of failure surface was determined based on our test results and Tani & Ueta (1991). The FEM mesh is shown in Figure 4a.

Solid elements were modeled based on the cap model (Chen & Baladi, 1985). Associated flow rule was used. In order to avoid numerical difficulties due to singularities in Mohr-Coulomb hexagonal pyramid in principal stress space, Drucker-Prager criterion was used as a failure criterion. This failure envelope is described by

$$h(I_1, \sqrt{J_2}) = \sqrt{J_2} - \alpha I_1 - k \qquad (1)$$

where I_1 is the first invariant of the stress tensor,

J_2 is the second invariant of the deviatoric stress tensor. α and k are material constants related to the frictional and cohesive strength.

The strain hardening elliptical cap is described by

$$H(I_1, \sqrt{J_2}, \kappa) = \sqrt{J_2} - 1/R\{[X(\kappa) - L(\kappa)]^2 - [I_1 - L(\kappa)]^2\}^{1/2} \qquad (2)$$

where R is the ratio of the major to the minor axis of the elliptic cap. $X(\kappa)$ and $L(\kappa)$ define the intersections of the elliptic cap with the I_1 axis and failure envelope (equation (1)), respectively. κ is the hardening parameter and is assumed to be

$$\kappa = \varepsilon_{kk}^p = W\{1 - \exp[-DX(\kappa)]\} \qquad (3)$$

where ε_{kk}^p is the plastic volumetric strain, W and D are material constants.

Initial vertical stress (σ_v) is assumed to be ρgh, where ρ is density, g is the acceleration of gravity and h is the depth. Horizontal stress (σ_h) is assumed to be $\nu/(1-\nu)\sigma_v$, where n is Poisson's ratio.

Initial shear modulus (G_0) is determined as follows. Ishida et al. (1981) described initial shear modulus of Gifu sand as a function of void ratio (e) and confining stress (σ_c)

$$G_0 = 1.42 \times 10^4 \frac{(2.17 - e)^2}{1 + e}(\sigma_c)^{0.321} \ (kN/m^2) \quad (4)$$

We modified equation (4) in order that the modulus calculated by equation (4) coincided with the one calculated by obtained density and shear velocity at the depth of 10cm.

Plane strain tests were performed to determine parameters. Internal friction angle of joint elements was obtained by peak stress. Cohesion is assumed to be 0Pa. Parameters of the cap model were determined by trial and error so that the calculated stress-strain curve fitted the curve obtained by the plane strain tests. Parameters used in our numerical analysis are listed in Table.1.
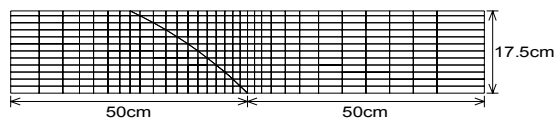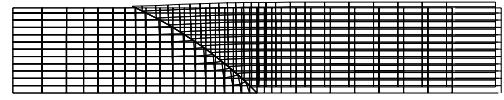
(a) FEM mesh
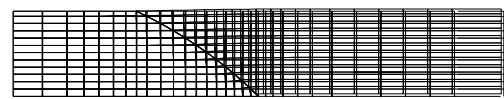
(b) vertical component of displacement 5mm
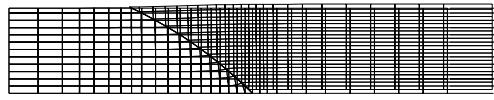
(c) vertical component of displacement 8mm

(d) vertical component of displacement 12mm

Figure 4: Result of FEM analysis

Figure 4b-d show the calculated deformation of the sand when the vertical component of the base fault displacement was 5mm (Fig. 4b), 8mm (Fig. 4c) and 12mm (Fig. 4d). In Figure 4b, relatively large deformation is observed in the lower region near the base fault, while the deformation near the ground surface is small and widespread. When the base fault displacement increases, we can distinguish the slip between the hanging wall and the footwall. In Figure 4c, slip can be seen in all joint elements. After formulating distinct slip throughout the sand, base fault displacement was consumed mostly by the slip in joint elements (Fig. 4d).

The joint element at the ground surface ruptured when the vertical component of the base fault displacement was 3.2mm. The relative vertical displacement of the joint element is less than 0.04mm in this case. When the vertical displacement of the base fault is 7mm, the relative vertical displacement of the joint element at the ground surface exceeds 1mm and the slip becomes distinct. This value is compatible with the result of our test (8mm).

The deformation of solid elements is large in the lower part near the failure surface of the footwall and small in the hanging wall side. The solid elements in the footwall side are dragged upward by the hanging wall. These two are compatible with the experimental result.

The slip in failure surface (joint elements) is large in shallow part compared to the test. This may be because we neglected the width of joint elements in our simulation while the shear failure surface has a certain width in real sand.

Our simulation can duplicate the test results generally well including the process of formulating shear failure surface and the process after it.
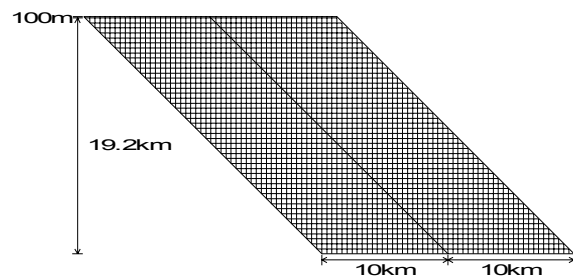

Figure 5: FEM mesh for bedrock fault analysis

3 APPLICATION OF NUMERICAL MODEL TO PROTOTYPIC REAL SCALE ALLUVIUM

We applied our numerical model to the prototypic real scale sandy alluvium and investigated the dynamic failure propagation in the alluvium. Our numerical analyses were divided into two parts. First, the dynamic movement of the bedrock fault was calculated by dynamic FE analyses. Then applying the obtained dynamic bedrock fault movement to the alluvium as a boundary condition, the failure process of the alluvium was calculated. The FE mesh for the dynamic bedrock fault analyses is shown in Figure 5. The joint elements are arranged along a potential fault plane. The dip angle is assumed to be 45 degree. The model consists of two layers. The upper one (100m) is the alluvium layer and the lower one (19.2km) is the bedrock layer. The density along with S wave velocity and Poisson's ratio of each layer are listed in Table 2.
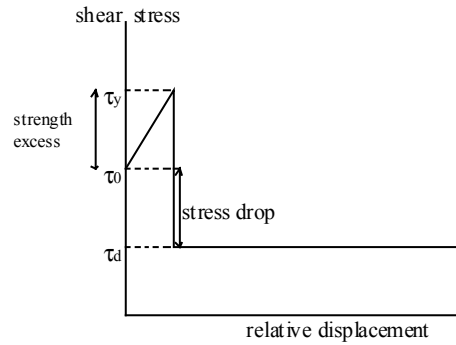
The shear stress-relative displacement relation of a joint element in the upper alluvium layer is assumed to be elastic-perfectly plastic (Fig. 6a). The assumed shear stress-relative displacement relation of joint elements in the bedrock is shown in Figure 6b. In Figure 6b, τ_0 and τ_d are the initial and the

Table 2: Parameters of bedrock – alluvium model

	Density	S wave velocity	Poisson's ratio
Alluvium	1.7g/cm^3	200m/s	0.3
Bedrock	2.5g/cm^3	3500m/s	0.25
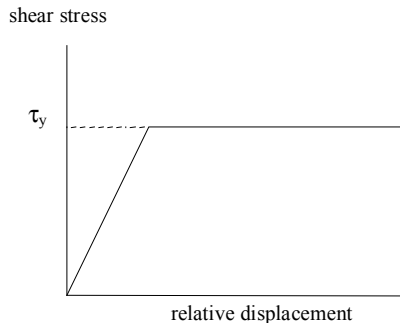
Figure 6a: Stress - relative displacement relation of alluvium joint elements

Figure 6b: Stress – relative displacement relation of bedrock joint elements

Table 3: Parameters of bedrock fault and result

|	Fault width	Stress drop	Strength excess	Vertical component of fault slip	Moment magnitude
Case1	19.2km	4.0MPa	4.7MPa	5.4m	7.33
Case2	19.2km	3.0MPa	4.0MPa	4.1m	7.25
Case3	19.2km	2.0MPa	2.5MPa	2.7m	7.20
Case4	19.2km	1.8MPa	2.5MPa	2.4m	7.17
Case5	19.2km	1.5MPa	2.0MPa	2.0m	7.12
Case6	9.6km	3.0MPa	4.0MPa	1.6m	6.60
Case7	9.6km	2.0MPa	2.5MPa	1.0m	6.48
Case8	9.6km	1.5MPa	2.0MPa	0.8m	6.40

residual stress, respectively. The strength excess is defined as the difference between the shear strength and the initial stress. The stress drop is defined as the difference between the initial stress and the residual stress.

When the shear stress in a joint element of the bedrock reaches the shear strength, it drops to the residual stress, which generates seismic wave. The shear stress in adjacent joint elements is increased by the seismic wave. If the stress in adjacent joint elements reaches the shear strength, the stress drop occurs and the rupture propagates. On the other hand, if the strength excess is high and the shear stress does not reach the shear strength, the rupture stops there.

Assigning different strength excess and stress drop in each joint element, eight different bedrock fault movements were calculated (case1-case8). Extremely high strength excess (100MPa) was assigned to lower joint elements and fault width was restricted to 19.2km (case 1-case 5) and 9.6km (case 6-case 8). Strength excess at the center of the

presumed bedrock fault was set to 0 and the rupture propagated bilaterally from the point. The bedrock fault movement was calculated for 25s with the time interval of 0.015s. Strength excess and stress drop are listed in Table 3 along with the vertical component of the final slip on the fault and the calculated moment magnitude.

The calculated bedrock movement was applied to the alluvium model as a boundary condition. In order to investigate the effect of the depth of the alluvium, four alluvium models with the depth of 30m, 50m, 75m and 100m were used. Joint elements were arranged along the potential shear failure surface. This failure surface was determined by Tani & Ueta (1991). The FEM meshes for these models are shown in Figure 7. The stress–relative displacement relation of joint elements was assumed to be elastic-perfectly plastic. The solid elements were assumed to be elasto-plastic and were modeled using the cap model. Parameters of the cap model were determined based on the plane strain tests performed in high confining stress (σ_3=392kPa)
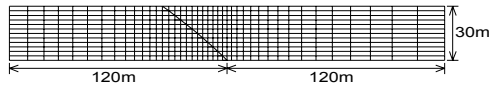
(a) 30m deep model
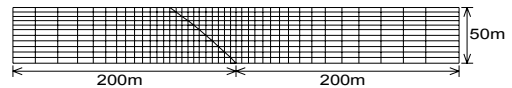
(b) 50m deep model
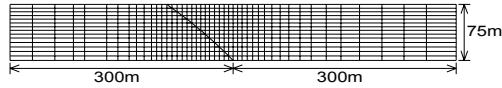
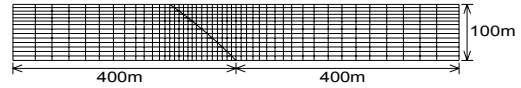(c) 75m deep model

(d) 100m deep model

Figure 7: FEM mesh for alluvium

Table 4: Parameters of numerical analyses

			Solid element	Joint element
Initial shear modulus			*1)	*1)
Poisson's ratio		ν	0.3	
Density			1.7g/cm3	
Parameters of Mohr-Coulomb criterion	Cohesion	C		0.0Pa
	Friction angle	φ		43.0 degree
Parameters of Drucker-Prager criterion		α	0.23	
		k	0.0Pa	
Hardening function parameters		D	$0.00009(kN/m^2)^{-1}$	
		W	0.05	
Major axis/minor axis		R	2.0	

*1) given by density and S wave velocity

(Park & Tatsuoka, 1994) (Tatsuoka et al., 1994). Parameters used in the alluvium analyses are shown in Table 4.

The vertical stress in joint elements and solid elements was assumed to be ρgh. The initial horizontal stress was assumed to be proportional to the vertical stress and two different conditions (0.4 times vertical stress and 0.7 times vertical stress) were considered. The initial shear modulus was calculated by the density and shear wave velocity, and two different velocity structures of the alluvium were assumed (constant velocity model and variable velocity model shown in Figure 8).

Applying dynamic bedrock fault movement to these alluvium models with different initial conditions, the shear failure of joint elements (potential shear failure surface) was investigated dynamically.

The shear failure propagated from lower part to upper part of joint elements. In some cases the failure propagated through the alluvium and broke the ground surface. In other cases it did not. Table 5 summarizes the simulation results. 'Y' indicates that the shear failure occurred in all of the joint elements. 'N' indicates that it did not. In 30m deep alluvium model, all joint elements in the alluvium ruptured
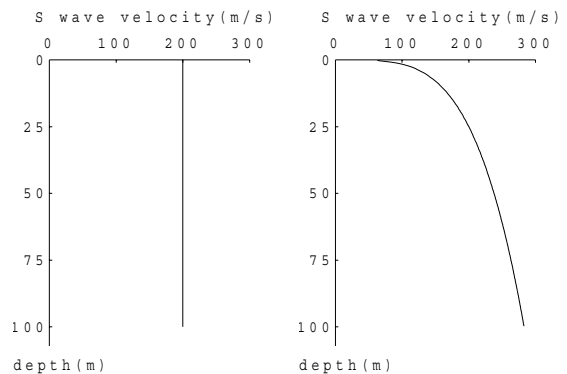
Figure 8: Assumed shear wave velocity structure of the alluvium

when the alluvium was subjected to the bedrock movement obtained in case 6. The vertical component of the bedrock fault slip is 1.6m, corresponding to 5.3% of the depth of the alluvium. In 50m deep alluvium model, all joint elements ruptured with 2.7m vertical slip of the bedrock fault, corresponding to 5.4% of the depth of the alluvium. Some joint elements did not rupture with 0.8m

Table 5: Results of numerical analyses

Depth of the alluvium	30m				50m				75m				100m			
Shear wave structure	Constant model		Variable model		Constant model		Variable model		Constant model		Variable model		Constant model		Variable model	
σ_h/σ_v	0.4	0.7	0.4	0.7	0.4	0.7	0.4	0.7	0.4	0.7	0.4	0.7	0.4	0.7	0,4	0.7
Case1									N	Y	N	Y	N	N	N	N
Case2									N	N	N	N				
Case3					Y	Y	Y	Y								
Case4					Y	Y	N	N								
Case5					N	N	N	N								
Case6	Y	Y	Y	Y												
Case7	Y	Y	N	N												
Case8	N	N	N	N												

vertical slip (2.7% of the depth) in 30m deep alluvium model and 2.0m vertical slip (4% of the depth) in 50m deep alluvium. The simulation result depends on the conditions of the alluvium when the alluvium was subjected to 1.0m vertical slip (3.3% of the depth) and 2.4m vertical slip (4.8% of depth) in 30m and 50m alluvium model respectively. In 75m alluvium model, some joint elements did not rupture with 4.1m vertical slip of the bedrock fault (5.5% of the depth of the alluvium). When the 75m deep alluvium was subjected to 5.4m vertical slip (7.2% of the depth of the alluvium), all joint elements ruptured in compressive initial stress state, while some joint elements did not rupture if the initial horizontal stress was assumed to be 0.4 times the vertical stress. More than 5.4m vertical slip was needed for all joint elements to rupture in 100m deep alluvium model.

Generally the failure propagated from lower part to upper part of joint elements, however because of low confining stress the failure at the ground surface occurred due to seismic wave before the shear failure reached to the ground. The slip in joint elements in this case was small and the slip in joint elements has become distinct after all joint elements ruptured.

The stress-strain curve of sand expands and shifts toward higher strain side as the confining stress increases. The shear failure strain becomes large with confining stress accordingly. This is the reason our numerical analyses show that more bedrock fault slip is needed to rupture joint elements for deeper alluvium model compared to the alluvium depth.

Since the rupture propagation in the alluvium over reverse fault is considered, the rupture in the alluvium is likely to occur in the compressive state of stress as shown in the 75m deep alluvium analyses. The constant shear velocity model gives higher shear modulus on the average in 30m and 50m deep alluvium model. The 30m and 50m deep alluvium analyses show that higher shear modulus makes the shear failure propagate more easily if the parameters of failure criteria are assumed to be independent of the shear modulus.

All joint elements did not rupture in our 100m deep alluvium model by the largest bedrock movement (case 1). The moment magnitude of case 1 is 7.33 and the obtained vertical slip 5.4m is large compared with its magnitude because we assumed large stress drop in the shallow part of the bedrock fault. Earthquakes of magnitude greater than 7.3 seldom occur in inland (intra plate). It is unlikely that the shear failure propagates through the 100m deep sandy alluvium.

5 CONCLUSIONS

We performed sandbox tests and numerical analysis of the tests to investigate the shear failure propagation in deposits by reverse faulting. The FE analysis using elato-plastic solid elements and joint elements to model shear failure surface can duplicate our test result generally well, if the stress-strain relation of the sand is properly modeled.

Applying the numerical model to the prototypic real scale sandy alluvium, the following conclusion has been obtained.
(1) The shear failure propagates through the sandy alluvium and breaks the ground surface if the vertical component of the bedrock fault slip reaches 3-5% of the depth of the alluvium regarding 30m and 50m deep alluvium. For 75m deep alluvium, vertical slip of about 7% of the depth of the alluvium is needed for shear failure to propagate through the alluvium. It is unlikely that the shear failure propagates through 100m deep alluvium.
(2) Compressive stress state and high shear modulus may help the shear failure propagate in alluvium over reverse fault.

REFERENCES

Bray, J.D., Seed, R.B. and Seed, H.B. [1994] "Analysis of earthquake fault rupture propagation through cohesive soil," *J. Geotech. Engrg.*, ASCE, **120(3)**, 562-580.

Chen, W.F. and Baladi, G.Y. [1985] "*Soil Plasticity*," Elsevier, New York.

Cole, D.A.Jr. and Lade, P.V. [1984] "Influence zones in alluvium over dip-slip faults," *J. Geotech. Engrg*, ASCE, **110(5)**, 599-615.

Ishida, T., Watanabe, H., Ito, H., Kitahara, Y. and Matsumoto, M. [1981] "Static and dynamic property of model test material (Gifu sand etc.) under low confining stress," *CRIEPI Report* (in Japanese).

Park, C.S., Tatsuoka, F. [1994] "Anisotropic strength and deformation of sands in plane strain compression," *Proc. XIII ICSMFE*, **1**, 1-4.

Roth, W.H., Kalsi, G. Papastamatiou, O. and Cundall, P.A. [1982] "Numerical modeling of fault propagation in soils," *Proc, 4 th Int. Conf. on Num. Meth. Geomech*, 487-494.

Scott, R.F. and Schoustra, J.J. [1974] "Nuclear power plant sitting on deep alluvium," *J. Geotech. Engrg*, ASCE, **100**, 449-459.

Tani K. and Ueta, K. [1991] "Shape and location of discontinuity in sand induced by fault displacement in bed rock," *Proc. 26 Japan National Conf. on Geotech. Engrg*, 1185-1188 (in Japanese).

Tani, K. [1994] "Numerical simulation of model test of reverse fault by FEM incorporating joint elements," *Proc. of Symposium on subsurface failure and localization of strain*, 215-222 (in Japanese).

Tatsuoka, F., Goto, S., Siddiquee, M.S.A., Yoshida, T., Kihata, Y. and Sato, T. [1994] "Deformation and strength characteristics of SLB sand and model testing method for Class-A prediction of model bearing capacity tests using a strip footing," *Proc. of Symposium on subsurface failure and localization of strain*, 1-8 (in Japanese).

Toki, K. and Miura, F. [1985] "Simulation of a fault rupture mechanism by a two-dimensional finite element method," *J. Phys. Earth*, **33**, 485-511.

Walters, J.V. and Thomas, J.N. [1982] "Shear zone development in granular materials," *Proc. 4th. Int.Conf. Num. Meth. Goemech.*, **I**, 263-274.